Electronic Structures of RTe_2 (R = La, Ce): A Clue to the Pressure-Induced Superconductivity in $CeTe_{1.82}$

J. H. Shim,[1] J.-S. Kang,[2] and B. I. Min[1]

[1]*Department of Physics, Pohang University of Science and Technology, Pohang 790-784, Korea*
[2]*Department of Physics, The Catholic University of Korea, Puchon 420-743, Korea*

(Received 28 April 2004; published 7 October 2004)

Electronic structures of RTe_2 (R = La, Ce) have been investigated by using the local spin density approximation (LSDA) and the LSDA + U (U: on-site Coulomb interaction) band methods. Both $LaTe_2$ and $CeTe_2$ show the very similar Fermi surface nesting features along the [100] direction, which drive the charge-density wave (CDW) instability in the Te(1) sheets. The contribution near E_F from Ce $4f$ states is negligible in agreement with the measured ARPES spectra. In the semimetallic CDW-distorted RTe_2, both Te vacancy and pressure induce the charge transfer from Te(1) $5p$ to R $5d$ states, producing the enhanced density of states at E_F. We suggest that these increased self-doped Te(1) $5p$ hole carriers are responsible for the pressure-induced superconductivity in nonstoichiometric $CeTe_{1.82}$.

DOI: 10.1103/PhysRevLett.93.156406 PACS numbers: 71.20.Lp, 71.18.+y, 74.70.Ad

One of the most interesting physical properties of $CeTe_2$ is the recent observation of the pressure-induced superconductivity [1] in $CeTe_{2-\delta}$ ($\delta = 0.18$) with $T_C = 2.7$ K, while stoichiometric $CeTe_2$ has an antiferromagnetic (AFM) ground state. $CeTe_2$ crystallizes in the layered Cu_2Sb-type tetragonal structure with two types of Te sites: Te(1) and Te(2). Te(1) atoms form the Te square sheet that is sandwiched by the corrugated double layers of Ce-Te(2) slabs. The isostructural $LaTe_2$ is reported to have the charge-density wave (CDW) instability along [100] direction in the ab plane that arises from the nesting between the electron and hole Fermi surfaces in the Te(1) square sheet [2,3]. $CeTe_2$ also reveals the pseudogap feature [4] and the superstructure [5], which are believed to be related to the CDW. Interestingly, the superconducting phase in $CeTe_{1.82}$ seems to coexist with the CDW and magnetic phases.

Because of the quasi-two-dimensional layered nature of $CeTe_2$, it shows strong anisotropic behavior in transport and magnetic properties. Upon cooling, the ab-plane resistivity and susceptibility indicate the insulator-to-metal (IM) transition at $T_{IM} = 5.8$ K and the AFM transition at $T_N = 4.3$ K. Neutron diffraction data were interpreted to represent the down-up–up-down ($ABBA$)-type AFM configuration along the c axis with the ferromagnetic (FM) Ce double layers above and below the Te(1) sheet [6]. In the presence of the magnetic field, a large negative magnetoresistance is observed, with a concomitant shift of T_{IM} toward higher temperature. To explain the anomalous transport and magnetic properties, the magnetic polaron picture was proposed [7,8].

The coexistence of the superconducting phase with the CDW phase in $CeTe_{2-\delta}$ is reminiscent of that in superconducting transition-metal dichalchogenides. For example, layered $2H$-$NbSe_2$ exhibits the incommensurate CDW transition below 35 K and the phonon-mediated superconductivity at $T_c = 7.2$ K. The superconducting carriers in $2H$-$NbSe_2$ are known to be Nb $4d$ electrons [9]. In contrast, neither the carrier type nor the origin of superconductivity in $CeTe_{2-\delta}$ has been clarified yet. Further, the effects of nonstoichiometric Te defects and pressure on the electronic structure of $CeTe_2$ have not been addressed.

In order to understand the underlying physics of $CeTe_2$ properly, it is essential to investigate its electronic structure systematically. In this Letter, we report the first-principles band structure results for $CeTe_2$. We have also studied the band structure of $LaTe_2$ for comparison. We used the linearized muffin-tin orbital (LMTO) band method with the atomic sphere approximation both in the local spin density approximation (LSDA) and the LSDA + U (U: on-site Coulomb interaction) band methods. The spin-orbit (SO) interaction was incorporated so that the orbital polarization is properly taken into account [10]. We included the valence-band muffin-tin orbitals up to f states for Ce and La, and up to d states for Te. Since $5p$ states of La and Ce are rather shallow, they are considered as valence states. To examine the CDW instability in RTe_2, we calculated their Fermi surfaces and susceptibilities. Then to investigate the effects of the CDW and Te vacancies on the electronic structures, we considered the distorted monoclinic $LaTe_2$ [$2 \times 2 \times 1$ supercell (8 f.u. of $LaTe_2$) with the $P1c1$ space group] which has the herringbone patterns [11], and the distorted tetragonal $CeTe_2$ [$2 \times 2 \times 2$ supercell (16 f.u. of $CeTe_2$) with the $P4$ space group] which has the double herringbone patterns [5]. We also estimated the superconducting parameters based on the rigid-ion approximation [12].

Figure 1 shows the band structure of $LaTe_2$, obtained by using the LSDA method, and that of $CeTe_2$, obtained by using the LSDA + U method. We considered the tetragonal structure for $LaTe_2$ with the lattice constants of $a = 4.56$ and $c = 9.12$ Å, and the doubled tetragonal structure along the c direction for $CeTe_2$ with $a = 4.47$ and $c = 18.22$ Å and the $ABBA$-type AFM configuration. The Ce $4f$ states in $CeTe_2$ are considered to be localized

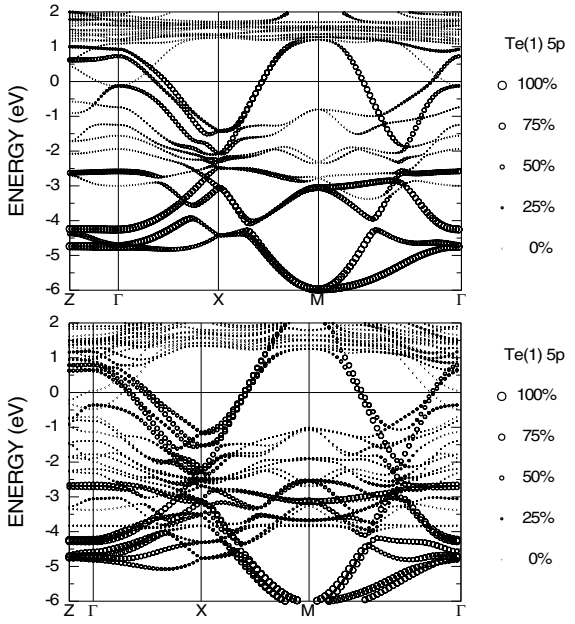

FIG. 1. The LSDA band structure of $LaTe_2$ (top) and the LSDA + U band structure of $CeTe_2$ (bottom). Γ, X, Z, and M represent the (0,0,0), (1/2, 0, 0), (0, 0, 1/2), and (1/2, 1/2, 0) $\mathbf{k}$ points in the simple tetragonal Brillouin zone. The size of the circle represents the contribution of the Te(1) $5p$ states in the wave function.

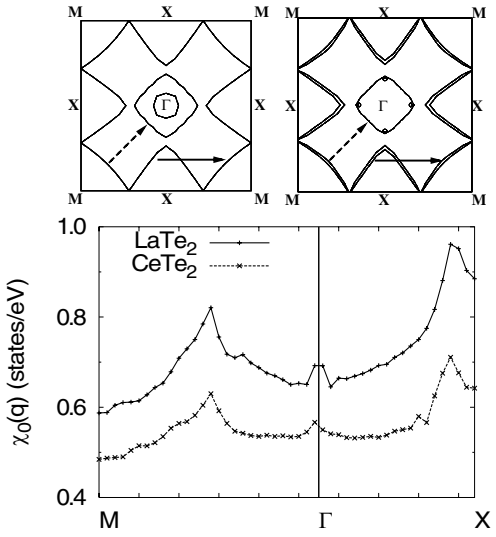

FIG. 2. Fermi surfaces of $LaTe_2$ (top left) and $CeTe_2$ (top right). The arrows correspond to the nesting vectors along the [100] and [110] directions. Bottom: Calculated susceptibilities for $LaTe_2$ and $CeTe_2$. $\chi_0(\mathbf{0})$ is normalized to DOS at E_F in each case.

far below E_F, which is supported by the angle-resolved photoemission spectroscopy (ARPES) data (Fig. 3). Thus the LSDA + U method will be more appropriate to describe the Ce $4f$ states than the LSDA method. We have used $U = 7$ eV and the exchange parameter $J = 0.95$ eV for Ce $4f$ electrons [13]. The overall shape of the band structure of $LaTe_2$ (top of Fig. 1) is similar to that in literature [3,11]. The highly dispersive bands crossing the Fermi level E_F are the Te(1) $5p$ states, which produce the large electron Fermi surfaces centered at X and the hole Fermi surfaces centered at Γ and M. The spin-orbit effect is negligible at the Fermi surfaces of Te(1) $5p$ bands. Figure 1 reveals that, except for Ce $4f$ bands, the band structure of $CeTe_2$ near E_F (bottom) is very similar to that of $LaTe_2$ (top). Therefore the Fermi surfaces of $LaTe_2$ and $CeTe_2$ are also very similar to each other and they produce the similar nesting feature.

Figure 2 compares the Fermi surfaces of $LaTe_2$ and $CeTe_2$. Both compounds show the very similar Fermi surface nesting of Te(1) $5p$ bands along the [100] direction. The CDW instability in the Te(1) sheet is driven by this nesting property [3]. The small difference between $CeTe_2$ and $LaTe_2$ is the location of the R $5d$ bands, which cross E_F near Γ: a small La $5d$ electron pocket centered at Γ is clearly seen for $LaTe_2$, whereas Ce $5d$ states near E_F are nearly degenerate with the Te(1) $5p$ states so as to show Γ-centered hybridized Fermi surfaces for $CeTe_2$. This difference is mainly due to the smaller volume for $CeTe_2$ than for $LaTe_2$. The smaller lattice constant for $CeTe_2$, especially in the ab direction, results in the larger direct R-R interaction so as to lower the Ce $5d$ bands near Γ point [11].

The nesting feature can be checked by examining the bare electronic susceptibility χ_0 that is obtained from the band structure output [14]:

$$\chi_0(\mathbf{q}) = \frac{1}{N}\sum_{n,n',\mathbf{k}} \frac{f(\epsilon_{n,\mathbf{k}})[1 - f(\epsilon_{n',\mathbf{k}+\mathbf{q}})]}{\epsilon_{n',\mathbf{k}+\mathbf{q}} - \epsilon_{n,\mathbf{k}}}, \qquad (1)$$

where $f(\epsilon)$ is the Fermi-Dirac distribution function, and $\epsilon_{n,\mathbf{k}}$ and $\epsilon_{n',\mathbf{k}+\mathbf{q}}$ are the eigenvalues at $\mathbf{k}$ and $\mathbf{k} + \mathbf{q}$ of the first Brillouin zone with the band indices n and n'. As shown at the bottom of Fig. 2, the calculated susceptibilities for both $LaTe_2$ and $CeTe_2$ indeed have peaks near X, which is consistent with the Fermi surface nesting along [100]. Smaller peaks are also seen near $\frac{1}{2}\Gamma M$, which is again consistent with the Fermi surface nesting along [110].

The top of Fig. 3 shows the bands having the Ce $4f$ character. The well localized Ce $4f$ bands are located at ~ -4.0 eV and at 1.0–2.5 eV. Noteworthy is the dispersive bands near Γ at ~ -1.0 eV with the Ce $4f$ contribution of ~20%, for which Ce $4f$ and Te(2) $5p$ states are strongly hybridized [15]. In addition, there is a convex band above E_F centered at M composed of Ce $4f$-Te(1) $5p$ hybridized states. However, the weight of Ce $4f$ states near E_F is rather low. The existence of the localized and dispersive Ce $4f$ bands is consistent with the ARPES spectra of $CeTe_2$, obtained from the Ce $4d \rightarrow 4f$ fine-structure resonance [16], shown at the bottom of Fig. 3. The angle θ_e labeled at each set of spectra denotes the emission angle in the ab plane along the lines parallel to the polarization of the incident light. The Ce $4f$ ARPES spectra show the typical two-peak structures, with the

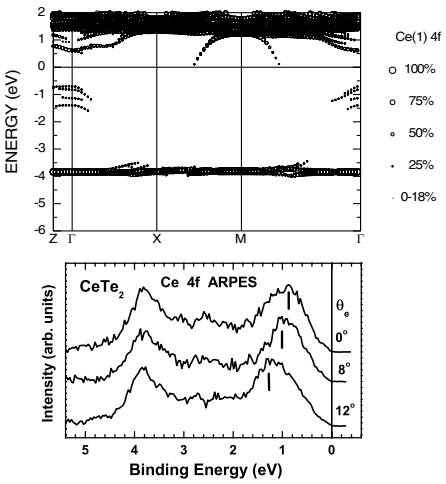

FIG. 3. Top: LSDA + U band structure of $CeTe_2$ with the Ce $4f$ contribution larger than 18%. Bottom: The extracted Ce $4f$ ARPES spectra of $CeTe_2$. These spectra were extracted from the Ce $4d \rightarrow 4f$ fine-structure resonance (Ref. [16]).

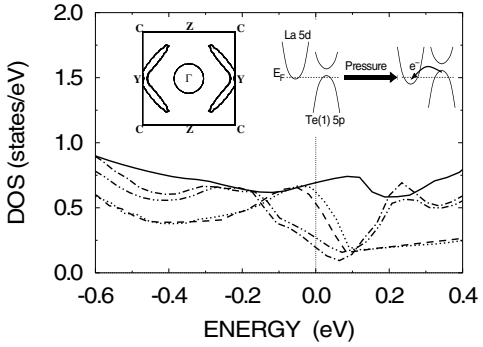

FIG. 4. The LSDA DOSs of tetragonal $LaTe_2$ (nondistorted) (solid), CDW-distorted $LaTe_2$ with the original (dot-dashed) and the reduced (double dot-dashed) volume, and CDW-distorted $LaTe_{1.75}$ with the original (dashed) and the reduced (dotted) volume, respectively. Left inset: Fermi surface of the CDW-distorted $LaTe_2$ with the original volume. Γ, Z, C, and Y represent (0,0,0), (0, 0, 1/2), (0, 1/2, 1/2), and (0, 1/2, 0) $\mathbf{k}$ points in the monoclinic Brillouin zone. Right inset: schematic diagram of the charge transfer from Te(1) $5p$ to R $5d$ states induced by the pressure.

lower binding energy (BE) peak around 1 eV, and the higher BE peak around 4 eV. The high and low BE peaks correspond to the $4f^0$ and $4f^1$ final-state peaks, respectively [17,18]. The low BE peak arises from the hybridization between the Ce $4f$ and valence-band electrons. It is observed that the low BE peak reveals a significant dispersion, while the high BE peak reveals no detectable dispersion. The dispersion of the low BE peak amounts to more than $\sim$300 meV between $\theta_e = 0°$ and $\theta_e = 12°$ [$\Delta k \approx 0.8(\frac{2\pi}{a})$]. The highly dispersive nature of Ce $4f$ states in $CeTe_2$ is consistent with the finding in the theoretical band structure, reflecting the strong hybridization between Ce $4f$ and Te(2) $5p$ states. Note also that the contribution near E_F from Ce $4f$ electrons is negligible, again in agreement with the theoretical band structure.

To investigate the effect of the CDW on the electronic structure of RTe_2, we have studied the electronic structures of the CDW-distorted $LaTe_2$ and $CeTe_2$. We have found that both compounds have the similar trends in density of states (DOS) near E_F. Hence we present in Fig. 4 the DOS of $LaTe_2$ only. For the CDW-distorted $LaTe_2$ (dot-dashed), the opening of the CDW gap is evident, i.e., the DOS near E_F is much suppressed as compared to that of the nondistorted $LaTe_2$ (solid). In fact, by the CDW arrangement in the Te(1) sheet, Te(1) $5p$ bands near E_F are split to have the energy gap of $\sim$0.2 eV. The lower Te(1) $5p$ band still crosses the Fermi level. On the other hand, the other states near E_F are hardly changed. Consequently the system is semimetallic even in the CDW phase. The left inset of Fig. 4 shows the corresponding Fermi surfaces for the CDW-distorted $LaTe_2$: the La $5d$ electron pocket at Γ and the boomerang-shaped hole Fermi surfaces of Te(1) $5p$ bands. These results are consistent with the observed metallic ground state of $LaTe_2$ [19].

By applying the pressure, the charge transfer occurs from the Te(1) $5p$ to the La $5d$ bands due to the upward and downward shifts of the Te(1) $5p$ and La $5d$ bands, respectively, as illustrated in the right inset of Fig. 4. The CDW-distorted $LaTe_2$ with the reduced lattice constant by 2% has the slightly enhanced DOS at E_F as compared to that with the original volume. Of course, the negative pressure yields the opposite behavior. With increasing the lattice constant by 4% (negative pressure), the CDW-distorted $LaTe_2$ shows the pronounced insulating behavior.

It is known that vacancies are easily formed in the Te(1) sheets. Hence we have investigated the electronic structure of nonstoichiometric $RTe_{1.75}$, where vacancies are regularly arranged on the well-separated specific Te sites in the Te(1) sheets [Te(11) sites in the Stöwe's notation [11]]. Here, too, we have considered the band structure of $LaTe_{1.75}$ for the computational simplicity. Te vacancy would play a role of electron doping. It turns out, however, that the simple rigid band scheme does not work. Because of the Te(1) vacancy, the band structure near E_F is drastically changed, that is, as shown by the dashed line in Fig. 4, the states above E_F mostly of Te(1) $5p$ character are suppressed and Te(1) $5p$ states at E_F are shifted up to induce the hole doping in Te(1) $5p$ bands. Another noteworthy feature is the localization of Te(1) $5p$ carriers which reduces the overall bandwidth of Te(1) $5p$ states by $\sim$10% and so increases the DOS at E_F. Hence the resulting DOS at E_F becomes higher than that of the CDW-distorted $LaTe_2$. The hole-doping process in the Te(1) sheet can also be controlled by pressure as in $LaTe_2$. Accordingly, the boomerang-shaped Te(1) $5p$ hole Fermi surface obtained for the CDW-distorted $LaTe_2$ becomes larger due to the Te vacancy and the positive pressure. We expect that these increased self-

doped Te(1) $5p$ hole carriers are responsible for the pressure-induced superconductivity observed in nonstoichiometric $CeTe_{2-\delta}$.

Note that the superconductivity in $CeTe_2$ is realized only for the nonstoichiometric Te-deficient sample under the pressure. So we have examined the superconducting properties for the CDW-distorted RTe_2 and the CDW-distorted nonstoichiometric $RTe_{1.75}$. Here, too, we used the band outputs for $LaTe_2$. Since the coexistence of superconductivity and the CDW phase indicates that the electron-phonon interaction plays some role, we have calculated the superconducting parameters within the rigid-ion approximation [12]. The electron-phonon coupling constant $\lambda_{\rm ph}$ is evaluated by employing the McMillan's formula [20], $\lambda_{\rm ph} = \sum_\alpha [N(E_{\rm F})\langle I_\alpha^2\rangle / M_\alpha \langle \omega_\alpha^2\rangle]$, where $\langle I_\alpha^2\rangle$ is the average electron-ion interaction matrix element for the αth ion, M_α is an ionic mass, and $\langle \omega_\alpha^2\rangle$ is the relevant phonon frequency. We have used the average phonon frequency $\langle \omega^2\rangle \simeq \Theta_D^2/2$, where Θ_D is the Debye temperature. The main contribution to $\langle I_\alpha^2\rangle$ comes from Te(1) $5p$ electrons. By using the experimental value of $\Theta_D \sim 128$ K, we get $\lambda_{\rm ph} = 0.15$ and $\lambda_{\rm ph} = 0.57$, for $LaTe_2$ and $LaTe_{1.75}$, respectively. Then the McMillan's formula for T_c with an effective electron-electron interaction parameter $\mu^* = 0.13$ yields $T_c = 0.0$ and $T_c = 1.4$ K, respectively. This result suggests that nonstoichiometry is very important. We can expect that the additional pressure effect would enhance the superconductivity. Indeed with the lattice constant contracted by 2%, $\lambda_{\rm ph}$ and T_c are enhanced to 0.71 and 2.9 K, respectively. We note that these enhancements arise not only from the change of bandwidth at E_F but also from the hole-doping process in the Te(1) sheets, as discussed in Fig. 4. The calculated value of $T_c = 2.9$ K for pressurized $LaTe_{1.75}$ is in reasonable agreement with the experimental value of $T_c = 2.7$ K of $CeTe_{1.82}$.

One important issue to be resolved is how superconductivity in $CeTe_{1.82}$ coexists with magnetism. The assumed *ABBA*-type AFM configuration for $CeTe_2$ would hinder the singlet superconductivity in the Te(1) sheets. More plausible in this environment would be the triplet pairing interaction for $CeTe_2$, mediated by the ferromagnetic fluctuations. However, the extreme sensitivity to the Te vacancy reflects that the magnetic fluctuation will not be the primary source of the pairing interaction [1]. The following reasons can be invoked to support the singlet superconductivity in $CeTe_2$. First, if the exchange interaction between Ce $4f$-Te(1) $5p$ states is weak, the singlet superconductivity would survive even in the magnetic phase, similarly as in a magnetic superconductor $ErRh_4B_4$. Indeed the band structure of $CeTe_2$ (shown in Fig. 2) manifests the rather weak hybridization between Ce $4f$ and Te(1) $5p$ states near E_F. This hybridization would be suppressed further by the opening of CDW gap at E_F. Second, if the magnetic moments of Ce ions surrounding the Te(1) sheets are antiferromagnetically aligned, the singlet superconductivity would be possible in the magnetic phase. The observed metamagnetic transition [21] at a very low magnetic field, $H = 700$ Oe, implies that the stability of the *ABBA*-type AFM configuration is not very strong. We have found the negligible total energy difference between the *ABBA*-type AFM configuration and other AFM configurations in which the surrounding Ce-Te layers are antiferromagnetically coupled, i.e., the *ABBA* type is lower in energy than the *ABAB* or *AABB* type by only $\lesssim 5$ meV/f.u., indicating that the stability of the *ABBA*-type AFM configuration is not so strong. Therefore one can speculate that, upon cooling, the AFM configuration in $CeTe_{1.82}$ is easily changed to become compatible with the singlet superconductivity. These reasons remain to be checked carefully by experiment.

This work was supported by the KRF (KRF–2002-070-C00038) and by the KOSEF through the eSSC at POSTECH and the CSCMR at SNU. Helpful discussions with S.J. Youn, U.-J. Yu, Y. S. Kwon, and M. H. Jung are greatly appreciated.

[1] M. H. Jung *et al.*, Phys. Rev. B **67**, 212504 (2003).
[2] E. DiMasi *et al.*, Phys. Rev. B **54**, 13 587 (1996).
[3] A. Kikuchi, J. Phys. Soc. Jpn. **67**, 1308 (1998).
[4] M. H. Jung *et al.*, Phys. Rev. B **63**, 035101 (2001).
[5] K. Stöwe, J. Alloys Compd. **307**, 101 (2000).
[6] J.-G. Park *et al.*, Physica (Amsterdam) **241B**, 684 (1997).
[7] M. H. Jung *et al.*, J. Phys. Soc. Jpn. **69**, 937 (2000).
[8] T. Kasuya *et al.*, J. Magn. Magn. Mater. **220**, 235 (2000).
[9] T. Yokoya *et al.*, Science **294**, 2518 (2001).
[10] S. K. Kwon and B. I. Min, Phys. Rev. Lett. **84**, 3970 (2000).
[11] K. Stöwe, J. Solid State Chem. **149**, 155 (2000).
[12] G. D. Gaspari and B. L. Gyorffy, Phys. Rev. Lett. **28**, 801 (1972).
[13] These parameters give the best agreement between calculated and measured Ce $4f$ spectra.
[14] In our calculation, we have approximated the oscillator strength of the matrix element to be constant.
[15] The feature of Ce $4f$ states at ~ -1.0 eV was also observed in the optical spectra by M. H. Jung *et al.*, Physica (Amsterdam) **230B–232B**, 151 (1997).
[16] J.-S. Kang, C. G. Olson, and Y. S. Kwon (unpublished).
[17] B. I. Min *et al.*, Phys. Rev. B **33**, 8005 (1986).
[18] J. W. Allen *et al.*, Adv. Phys. **35**, 275 (1987).
[19] B. H. Min *et al.*, Physica (Amsterdam) **312B–313B**, 205 (2002).
[20] W. L. McMillan, Phys. Rev. **167**, 331 (1967).
[21] B. H. Min *et al.*, Physica (Amsterdam) **312B–313B**, 203 (2002).